5A.8   IDENTIFYING NONSTATIONARITY IN THE ATMOSPHERIC SURFACE LAYER

Edgar L Andreas[*,1], Cathleen A. Geiger[1], George Treviño[2], and Kerry J. Claffey[1],

[1]U.S. Army Cold Regions Research and Engineering Laboratory, Hanover, New Hampshire
[2]CHIRES, Inc., San Antonio, Texas

1. INTRODUCTION

The atmospheric boundary layer is inherently nonstationary. The sun rises and sets. Fair-weather clouds pass overhead and periodically shade the surface. Thicker, more extensive cloud layers provide even more shading during daylight hours and act as a blanket against radiative cooling at night. But the transition in sky conditions as these cloud layers develop or dissipate rapidly forces the surface temperature just as do fair-weather clouds and sunrise and sunset transitions.

The lower atmosphere responds almost immediately to this rapid surface forcing because the forcing manifests first as a change in surface temperature. The surface temperature, in turn, feeds into the sensible and latent heat fluxes, which affect the near-surface atmospheric temperature and humidity profiles in short order. A change in the sensible heat flux also alters the near-surface atmospheric stratification and, thus, quickly influences the wind speed profile.

Monin-Obukhov similarity theory, which organizes our understanding of the atmospheric boundary layer—especially the atmospheric surface layer—relies on two assumptions that seem at odds with this depiction of the atmospheric boundary layer: that the atmosphere is statistically stationary and that the surface is horizontally homogeneous. In fact, in some cases, the nonstationarity and the horizontal inhomogeneity go hand-in-hand, even when the surface looks visually homogeneous. For example, anyone who had flown over the U.S. Great Plains on a late-summer day featuring fair-weather cumulus may have noticed the light and dark patches that the cloud shadows create on the uniformly brown surface. Surface temperatures in the cloud shadows can be 5–10°C cooler than in full sunlight. Hence, a meteorological tower fixed on the surface would experience the nonstationarity of the passing clouds but also the horizontal inhomogeneity caused by the resulting variability in surface temperature (cf. Roth and Oke 1995).

Because clouds are ubiquitous, we speculate that many of the measurements of the Monin-Obukhov similarity functions that have been reported were collected in nonstationary conditions. Such violations of the premises on which Monin-Obukhov similarity rests may explain some of the scatter that still exists in these "universal" similarity functions despite almost 50 years of measurements to quantify them (e.g., Högström 1996; Andreas et al. 1998; Johansson et al. 2001; Andreas 2002; Klipp and Mahrt 2004).

Still, the measured Monin-Obukhov similarity functions are not wildly scattered—just perplexingly scattered. Hence, perhaps the need for stationary conditions is not a strong constraint on Monin-Obukhov similarity theory. Our premise here, though, is that we know so little about how to handle or even to judge nonstationarity that we cannot make progress in determining its consequences without a better way to characterize it.

Foken and Wichura (1996), Vickers and Mahrt (1997), Mahrt (1998), and Andreas et al. (2003), among others, have described methods for identifying nonstationarity in atmospheric boundary layer time series. But these three groups alone describe at least five methods for identifying nonstationarity—for example, comparing statistics from short series to statistics from longer series, computing trends, counting zero crossings, and using information in the probability density function. That is, the community has reached no consensus on how to identify—let alone deal with—nonstationary.

Here we present yet another method for identifying nonstationarity, but our method has three advantages: It has a theoretical basis, it

---

[*]*Corresponding author address:* Edgar L Andreas, U.S. Army Cold Regions Research and Engineering Laboratory, 72 Lyme Road, Hanover, New Hampshire 03755-1290; e-mail: eandreas@crrel.usace.army.mil.

Report Documentation Page

1. REPORT DATE **2007**	2. REPORT TYPE	3. DATES COVERED **00-00-2007 to 00-00-2007**

4. TITLE AND SUBTITLE	5a. CONTRACT NUMBER
Identifying Nonstationarity in the Atmospheric Surface Layer	5b. GRANT NUMBER
	5c. PROGRAM ELEMENT NUMBER
6. AUTHOR(S)	5d. PROJECT NUMBER
	5e. TASK NUMBER
	5f. WORK UNIT NUMBER

7. PERFORMING ORGANIZATION NAME(S) AND ADDRESS(ES) **U.S. Army Cold Regions Research and Engineering Laboratory,Hanover,NH,03755**	8. PERFORMING ORGANIZATION REPORT NUMBER

9. SPONSORING/MONITORING AGENCY NAME(S) AND ADDRESS(ES)	10. SPONSOR/MONITOR'S ACRONYM(S)
	11. SPONSOR/MONITOR'S REPORT NUMBER(S)

12. DISTRIBUTION/AVAILABILITY STATEMENT
Approved for public release; distribution unlimited

13. SUPPLEMENTARY NOTES
Preprints, 21st Conference on Hydrology, San Antonio, TX, 14?18 January 2007, American Meteorological Society, in press

14. ABSTRACT

15. SUBJECT TERMS

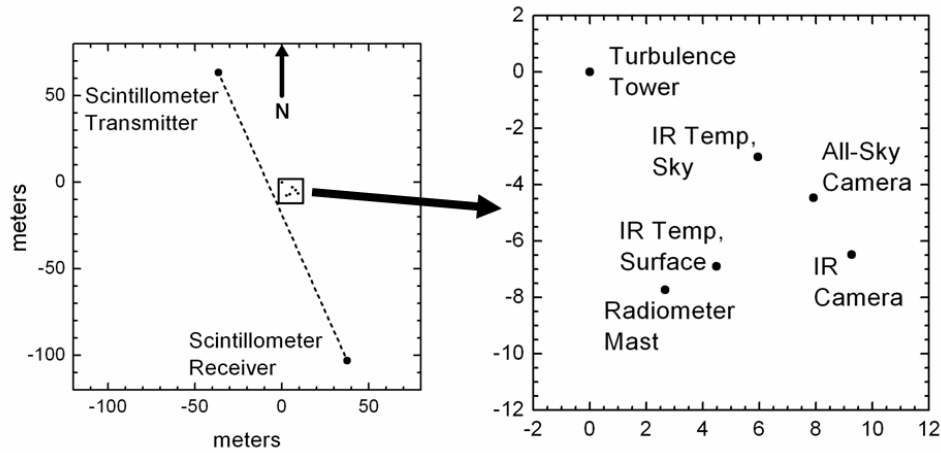| 16. SECURITY CLASSIFICATION OF:			17. LIMITATION OF ABSTRACT	18. NUMBER OF PAGES	19a. NAME OF RESPONSIBLE PERSON
a. REPORT **unclassified**	b. ABSTRACT **unclassified**	c. THIS PAGE **unclassified**	**Same as Report (SAR)**	**12**	

Fig. 1. Instrument layout for our April 2005 experiment. The "Turbulence Tower" is at the origin of our experimental grid.

relies on accepted definitions of what constitutes nonstationarity, and it associates a probability as to whether any nonstationary period it identifies is truly nonstationary.

Averaging a nonstationary time series is a fundamental problem because, by definition, the resulting statistics depend on when you begin to average and how long you average. We average using Treviño and Andreas's (2000) Time Dependent Memory Method (TDMM), which was formulated especially to pull out the mean and turbulent fluctuations from a nonstationary series. We then invoke Priestley's (1981) definitions of first-order and second-order nonstationarity and use standard statistical functions to test for first-order and second-order nonstationarity. These functions also help us assign significance levels to these tests.

The data we use in these analyses come from a dedicated experiment during which we combined a suite of radiation instruments to characterize forcing by sun, sky, and clouds and the surface's response to this forcing with turbulence instruments to document the concomitant near-surface atmospheric response to this forcing. Our analysis reveals nonstationarity in the near-surface air temperature and humidity associated with rapid changes in sky conditions. Andreas et al. (2006) have reported some of our preliminary results.

2. MEASUREMENTS

The data we use in our analysis come from a two-week experiment conducted in a 15-acre field in Lebanon, New Hampshire, in April 2005. The field had been mowed the previous fall and was, thus, covered in grass stubble and clippings a few centimeters thick. When the experiment began, the grass was dormant and the ground was cold, with the soil still frozen a few centimeters below a thawed surface layer. The grass greened up noticeably by the end of the experiment, however, but was still short.

Figure 1 shows our experimental layout and our main instrument cluster.

We used Eppley hemispherical, broadband longwave (model PIR) and shortwave (model PSP) radiometers to measure incoming and outgoing longwave and shortwave radiation. We also used Heitronics infrared thermometers to measure the sky (KT 19.85II, wavelength 9.6–11.5 μm) and surface (KT 19.81II, wavelength 8–10 μm) temperatures. These are narrow-beam radiometers; they have a 2.5° field of view. Our last radiation instrument was a Thermoscan model S60 digital infrared camera from FLIR Systems. This operates in the 7.5–13 μm wavelength band and has 76,800 pixels in its field of view.

We sampled the Eppley radiometers and the Heitronics thermometers at 1 Hz and will concentrate on this rapidly sampled data in our analysis. We obtained an image from the infrared camera once a minute and averaged over its

entire field of view to get the average surface temperatures we show soon.

Later, we will show temperatures obtained by converting the longwave radiation (Q_L) from both the Eppley up-looking and down-looking instruments to a blackbody temperature using

$$T_{BB} = \left(Q_L / \sigma\right)^{0.25} . \qquad (1)$$

This gives T_{BB} in kelvins when Q_L is in $W\,m^{-2}$, where σ ($=5.670400\times10^{-8}\,W\,m^{-2}\,K^{-4}$) is the Stefan-Boltzmann constant.

Near these radiation instruments, we had a "turbulence" tower with a three-axis, K-type sonic anemometer/thermometer from Applied Technologies Inc. (Kaimal et al. 1990; Kaimal and Gaynor 1991; Kaimal and Finnigan 1994, p. 218f.) mounted 3.6 m above the surface. Placed just below the sonic (Kristensen et al. 1997) was a Li-Cor 7500 fast-responding water vapor and carbon dioxide sensor. We sampled all of these instruments at 10 Hz. In the following plots, though, we show times series of these turbulence signals subsampled at 1 Hz simply for convenience.

For the possibility of putting these point measurements in a larger spatial context, we deployed a surface-layer scintillometer system (SLS20 from Scintec Atmosphärenmesstechnik GmbH) over a 182-m path such that our point instruments were near the center of the propagation path. The scintillometer measures the refractive index structure parameter and the inner scale of turbulence with 1-minute averaging (Andreas et al. 2003).

Finally, we documented sky conditions with periodic pictures from an all-sky camera (Nikon Coolpix 4500 with a Nikon fisheye converter lens).

3. QUANTIFYING THE NONSTATIONARITY

One of the central issues in atmospheric turbulence is deciding how long to average a turbulence time series to obtain meaningful estimates of the mean, the variance, and the turbulent fluxes (e.g., Lumley and Panofsky 1964, p. 35ff.; Wyngaard 1973; Sreenivasan et al. 1978; Andreas 1988; Lenschow et al. 1994). Most attempts to answer this question implicitly assume that the turbulence time series is stationary. But in light of the host of time scales represented in the forcing that we described in the Introduction, we believe that an analysis based on assuming nonstationarity may be more realistic.

Turbulence analyses typically begin with an instantaneous measurement of some variable $\tilde{x}$ (e.g., the longitudinal wind component). The purpose of averaging is to separate this instantaneous value into mean (X) and turbulence (x) components such that

$$\tilde{x} = X + x , \qquad (2)$$

where the average of x is zero. When a series is nonstationary, however, the mean of $\tilde{x}$ may not be approximately constant over typical hour-long averaging periods; X is thus ill-defined. The average magnitude of x may also vary. We show both manifestations of nonstationarity in our later figures.

Treviño and Andreas (2000), however, developed a rational way to separate the mean and the fluctuations, as required in (2), in a turbulence series that is assumed to be nonstationary. The method applies equally well to stationary series, too, though. Treviño and Andreas call their technique the Time Dependent Memory Method (TDMM; U.S. Patent No. 6,442,506) because it finds two time scales for averaging. One scale—call it ΔT—defines an averaging window over which to compute the mean (i.e., X) and, in turn, to separate the turbulent part (i.e., x). Finding ΔT requires that we specify the measurement accuracy and invoke the constraint that we cannot know something to better precision than our measurement accuracy.

A second time scale, the 'memory,' L, derives as the decorrelation time implied by the autocorrelation function of the turbulent part; it is essentially an integral scale. Treviño and Andreas (2000) then take $10L$ as the averaging window over which to compute the variance, $\sigma^2 = \overline{x^2}$, where the overbar indicates a time average. Using $10L$ as the window for computing σ^2 provides an adequate number of independent samples. Usually, $10L$ is computed to be less than ΔT; if it is not, we set the averaging time for computing variance to ΔT.

Using this method to choose proper averaging times—even when the series is nonstationary—we can compute the mean and variance along steps through that series and can test whether the series is stationarity or nonstationary. Priestley (1981, p. 104ff.) describes the concept of a process that is stationary at order m. If a process is order-1 (first-order) stationary, its mean does not change with

time. If a process is order-2 (second-order) stationary, its variance does not change with time.

Under the hypothesis that the mean is constant, the statistic

$$t = \frac{X_i - X_{i+1}}{\left[\dfrac{\sigma_i^2}{n_{i+1}} + \dfrac{\sigma_{i+1}^2}{n_i}\right]^{1/2}}\left[\frac{n_i + n_{i+1} - 2}{n_i + n_{i+1}}\right]^{1/2} \quad (3)$$

has a Student's t distribution with zero mean, variance 1, and $n_i + n_{i+1} - 2$ degrees of freedom. Here, X_i and X_{i+1} and σ_i^2 and σ_{i+1}^2 are the means and variances of adjacent intervals in a turbulence time series, computed using TDMM, and n_i and n_{i+1} are the number of independent samples used to compute the variances. By computing t, we can test for first-order nonstationarity.

We compute X_i and σ_i every 30 seconds to ensure that adjacent values are independent and to have a reasonable number of degrees of freedom for each estimate. We have estimated the integral scale for our turbulence data to be $3 - 4\,s$. Hence X_i values separated by 30 s are based on at least 10 independent samples. We also set the minimum averaging time ΔT as 30 s, though it was usually computed to be longer. Thus, in the above t statistic, both n_i and n_{i+1} are at least 10, and t has at least 18 degrees of freedom. If $|t|$ is larger than 2.878, then, the series is first-order nonstationary at the 1% significance level.

Likewise, the statistic

$$F = \frac{n_i \sigma_i^2 (n_{i+1} - 1)}{n_{i+1} \sigma_{i+1}^2 (n_i - 1)} \quad (4)$$

has an F distribution with $n_i - 1$ and $n_{n+1} - 1$ degrees of freedom. By computing F for adjacent intervals, we can test for second-order nonstationarity.

The Time Dependent Memory Method uses 10L as the averaging window for variance. That is, each variance estimate derives from approximately 10 independent samples since L is approximately the instantaneous correlation time of the series. Hence, again, n_i and n_{i+1} are both 10 in (3) and (4). Moreover, the F statistic reduces to $\sigma_i^2 / \sigma_{i+1}^2$; and in the F distribution, both degrees of freedom are 9. Therefore, the 99% confidence interval for F in (4) is $[0.153, 6.54]$. F values outside this interval indicate that a time series is second-order nonstationary at the 1% significance level.

4. RESULTS

Here we consider just two days from our experiment to demonstrate the various types of rapid forcing and to investigate nonstationarity.

Figure 2 shows time series from 26 April 2005 of incoming shortwave radiation, surface temperature inferred from the down-looking Eppley radiometer, sky temperature from the up-looking infrared thermometer, and air temperature from the sonic thermometer. On a clear day, the shortwave trace is very smooth, with a peak near 1000 W m^{-2} around noon. On 26 April, though, thin cirrus before noon and cirrus and cirrostratus after noon blocked the sun to varying degrees. The sky temperature reiterates the presence and effects of these clouds. A warming sky indicates increasing clouds, while a cooling sky signals dissipating clouds. Between midnight and 0400 hours, in fact, the sky and surface temperatures were nearly the same: Clouds were so thick that the surface and the clouds were nearly in radiative equilibrium.

The forcing by these clouds and, especially, the change in forcing, is almost immediately evident in the surface temperature and in the air temperature. For example, under the thick clouds between midnight and 0400 hours, the air temperature shows very small turbulent fluctuations. But when these clouds begin clearing, the surface temperature falls by about 5°C, and the air temperature likewise cools a degree or two. Moreover, the air temperature trace shows large fluctuations, evidence of downward sensible heat transfer to offset the surface cooling.

During the day, you can follow ripples in the incoming shortwave radiation and sky temperature in Fig. 2 through the surface temperature and the air temperature. The spiky shortwave trace implies that the cloud forcing can change quite rapidly, but the surface and air temperatures respond almost immediately.

Just one example of this daytime forcing in Fig. 2 is the persistent cloud from about 1500 to 1700 hours. As soon as evidence of the cloud appears in the shortwave and sky traces in the figure, the surface temperature begins falling from a local maximum near 1500 hours and falls almost 15°C while the cloud lasts. The air temperature
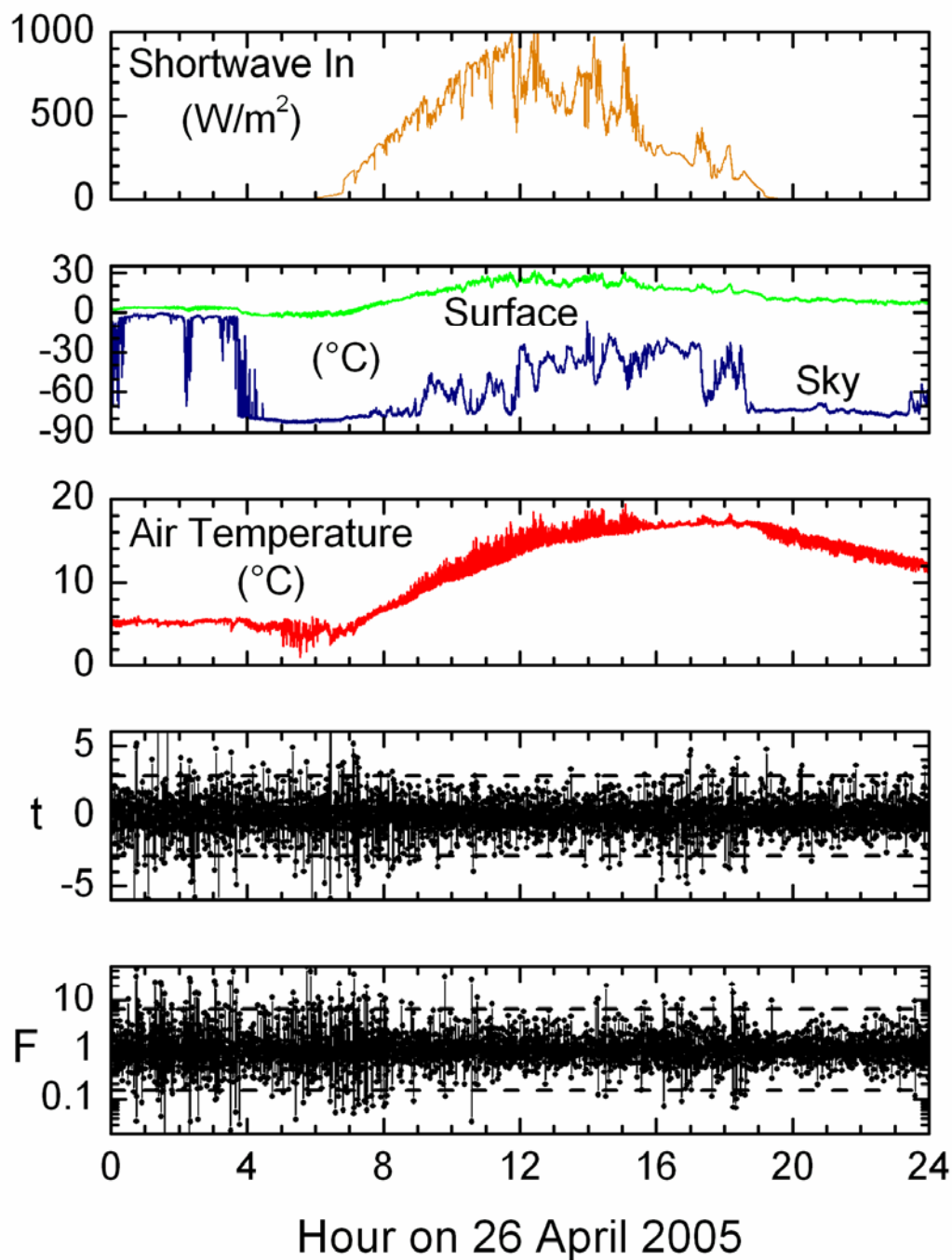
Fig. 2. Time series for all of 26 April 2005 of incoming shortwave radiation, blackbody surface temperature from the down-looking Eppley radiometer, sky temperature from the up-looking infrared thermometer, and air temperature from the sonic thermometer. All of these traces are 1-Hz data. The lower two panels are t and F statistics computed every 30 s from (3) and (4) from the raw 10-Hz temperature data; horizontal dashed lines are 99% confidence limits.

follows suit almost immediately: The air temperature falls about 4°C, and the turbulent fluctuations decrease to nighttime levels.

The lower two panels in Fig. 2 show time series of the t and F statistics computed from the 10-Hz temperature data. An obvious feature of these two traces is that the first eight hours of the day show many more excursions of t and F outside their respective 99% confidence limits than during the rest of the day. These statistics, thus, confirm what most micrometeorologists already know: Conditions at night are often nonstationary. But the t and F statistics also highlight periods of nonstationarity during daylight hours that evidently result from cloud forcing. For example, the cloud between 1500 and 1700 hours affected air temperature enough to produce clusters of excursions beyond the 99% confidence limits in both t and F during this period.

Figure 3 shows several day-long time series from 22 April 2005. This day featured clear skies from midnight until 0900 hours, as evidence by our up-looking infrared thermometer ("Sky Temp.") seeing sky temperatures lower than its minimum instrumental range. Thin cirrus clouds, many from spreading contrails, then began forming. Next, thicker cirrostratus developed at about 1530 hours and intermittently blocked and revealed the sun until about 1800 hours. Finally, thicker clouds developed after sunset, as evidenced by the sky temperature.

Again, the forcing by clouds ripples quickly through the surface and air temperatures in Fig. 3. The clearest example is for the sequence between 1530 and 1800 hours, which was under the influence of cirrostratus clouds with four main clearing episodes. The two surface temperatures and the air temperature all show nearly instantaneous and significant cooling when the clouds encroach but also show warming coincident with the thinning or clearing events during this period. The water vapor trace also shows up-going spikes that correspond with these clearing events.

The cluster of lower water vapor densities centered at 1530 hours may also be associated with the arrival of this cloud. Likewise, the steep increase in water vapor density after 2000 hours seems correlated with the thick clouds that developed then.

Figure 4 shows the t and F statistics every 30 s for the temperature and water vapor traces depicted in Fig. 3. As with Fig. 2, we see in Fig. 4 a lot more excursions for t and F outside their

respective 99% confidence bands between midnight and 0800 hours than later in the day.

On this day, the F statistic, which quantifies changes in variance and, thus, second-order nonstationarity, seems to be a better indicator of cloud forcing than the t statistic. For example, the F statistic for both air temperature and water vapor density responds with excursions outside the 99% confidence band when clouds move in at about 1530 hours. The corresponding t statistic here, which quantities a change in the mean and, thus, first-order nonstationarity, increases a bit in magnitude but remains within the 99% confidence band at the start of the episode.

Lastly, we want to look more closely at the midnight-to-0800-hours period for 22 April and demonstrate that the t and F statistics have implications for the dynamics that govern the nonstationarity. Figures 5 and 6 combine the temperature and water vapor traces, respectively, from Fig. 3 with the t and F statistics from Fig. 4 for midnight to 0800 hours on 22 April. In these expanded plots, it is easier to see what behavior in the time series of the physical variable produces a large response in t or F. For example, any high peak or deep valley in the time series usually correlates with t or F excursions outside the 99% confidence bands. Likewise, any quiet period in the turbulence that is followed by a relatively noisy period, or vice versa, correlates with excursions in F. The deep, steep valley in air temperature (Fig. 5) at about 0600 hours, for instance, is an event that produces responses in both t and F. The rapid climb but decreasing variability in water vapor density (Fig. 6) for 0330 to 0430 hours is another event producing responses in both t and F.

Figures 7 and 8, respectively, show alternative presentations of the t and F statistics for temperature and water vapor density. Here we take the same information as in Figs. 5 and 6 but plot F versus t. These plots more clearly show how often the series are strictly stationary, first-order but not second-order nonstationary, second-order but not first-order nonstationary, and both first-order and second-order nonstationary.

In the t and F scatter plot for air temperature (Fig. 7), 111 of 959 samples show first-order nonstationarity. That is, these samples lie in sectors I–IV and b and d. Likewise, 179 of 959 samples show second-order nonstationarity. These samples lie in sectors I–IV and a and c. Since we are testing for first-order and second-order nonstationarity at the 1% significance level,
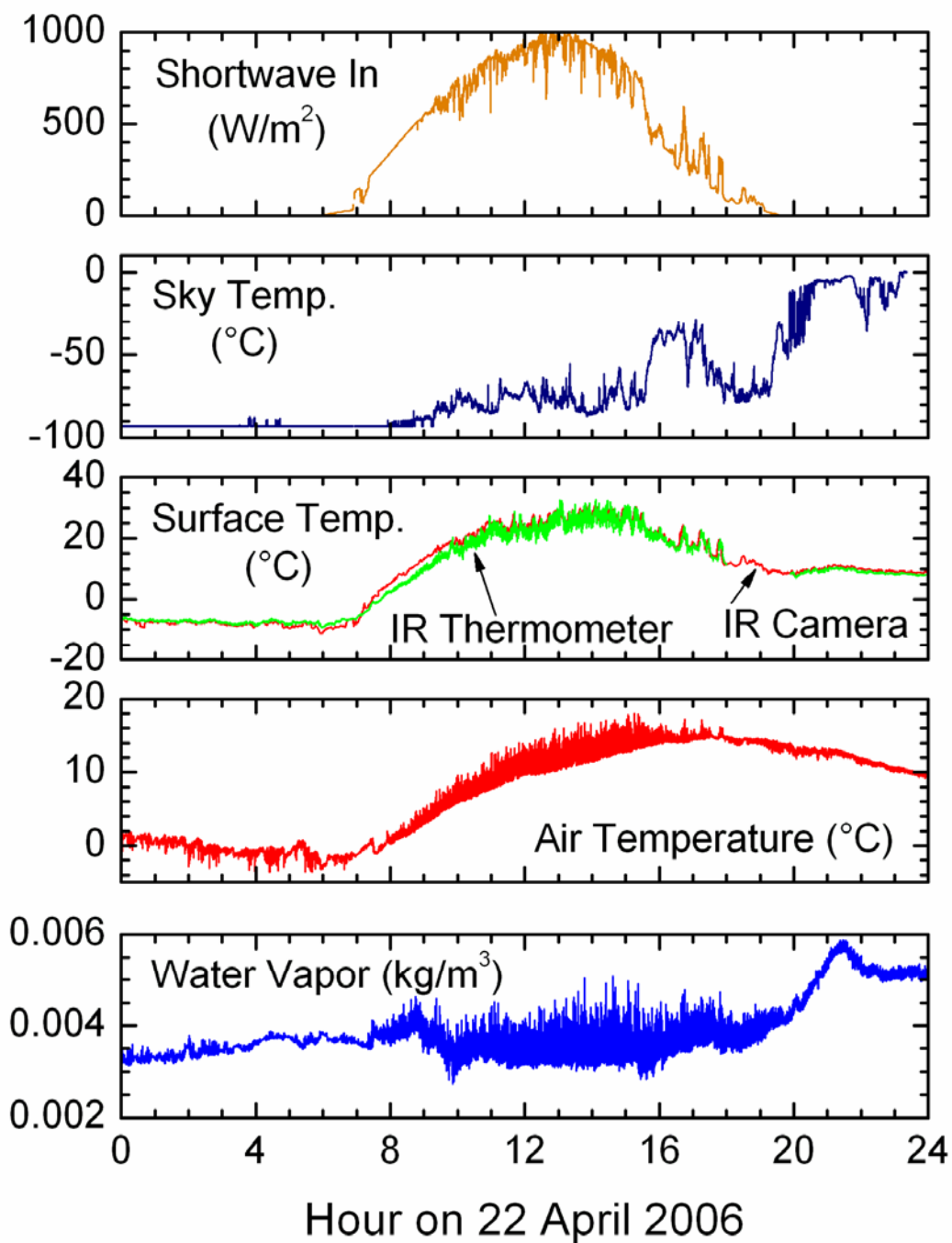
Fig. 3. Time series for all of 22 April 2005 of incoming shortwave radiation, sky temperature from the up-looking infrared thermometer, surface temperature measured by both the infrared camera and the down-looking infrared thermometer, air temperature measured by the sonic, and water vapor density measured by the Li-Cor 7500. All traces are 1-Hz data except the infrared camera, which sampled once a minute.
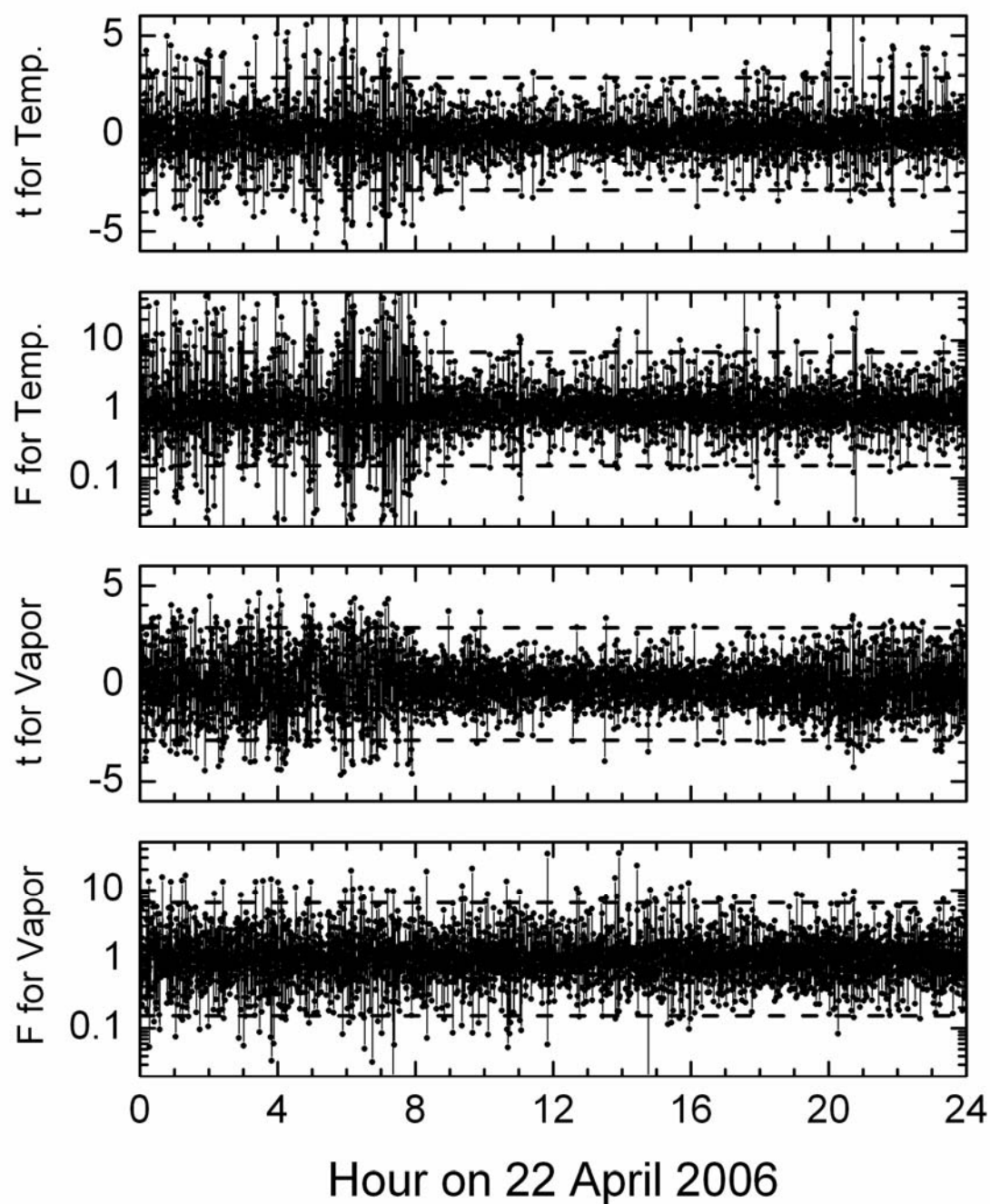
Fig. 4. The t and F statistics every 30 s computed using (3) and (4) and the raw 10-Hz data for the air temperature and water vapor series depicted in Fig. 3. The dashed lines are 99% confidence limits.
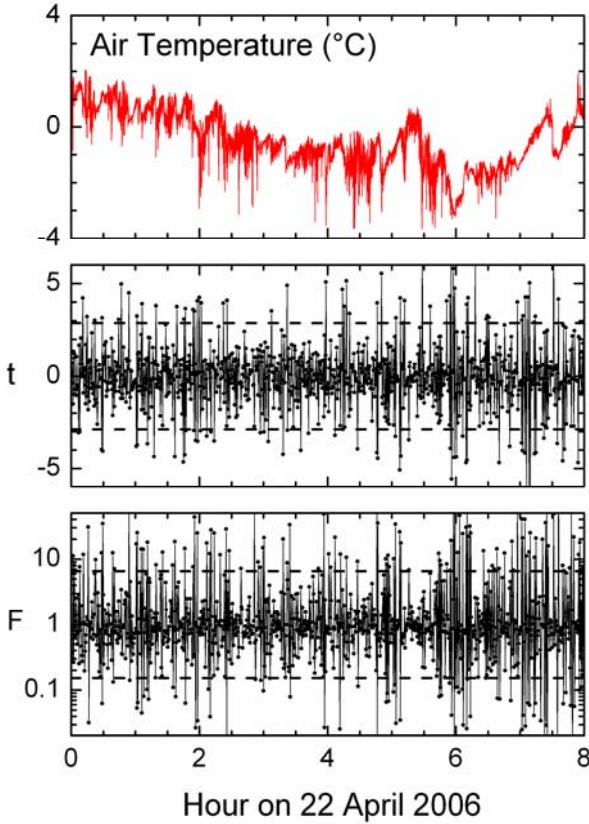
Fig. 5. Air temperature from midnight to 0800 hours on 22 April 2005 and corresponding t and F statistics at 30-s intervals. The dashed lines are 99% confidence limits.
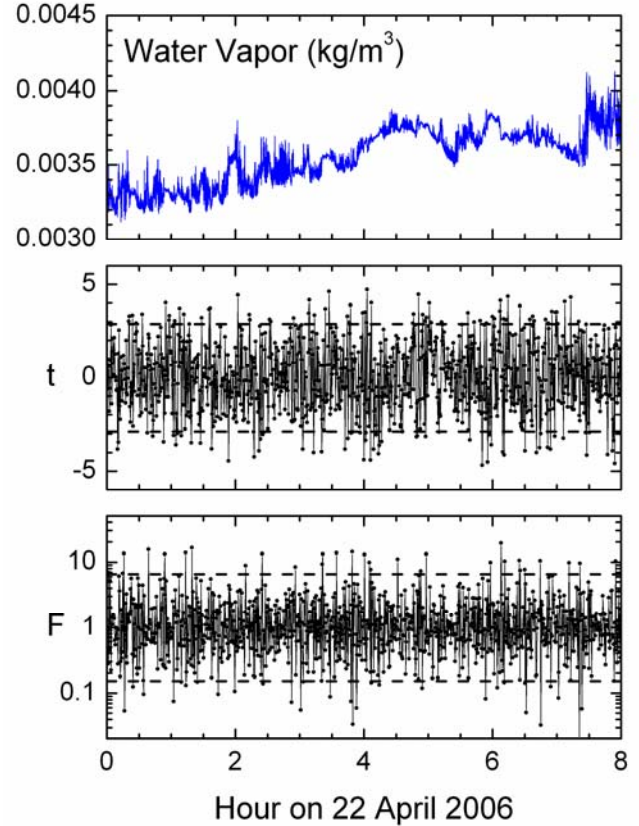

Fig. 6. As in Fig. 5, but this plot is for water vapor density.

we would expect only 10 t and 10 F values (i.e., 1% of 959 samples) to randomly fall outside the central box in Fig. 7 if the data were truly stationary. We can therefore easily conclude that the air temperature data for 0000 to 0800 hours on 22 April were nonstationary at either first order or second order.

A more restrictive test might be to call the data nonstationary only if they exhibit first-order and second-order nonstationarity simultaneously. In other words, only samples that fall in sectors I–IV would be indicators of a nonstationary time series. Still, however, in Fig. 7, 72 samples, 7.5% of the available data, fall in these sectors. Thus, even with this narrower definition of nonstationarity, the temperature trace in Fig. 5 would still be judged nonstationary.

Figure 7 also reveals something about the dynamics of the nonstationarity. Most of the samples that display both first-order and second-

order nonstationarity fall in sector IV. Here t is negative, and F is greater than one. From our definitions of t and F [see (3) and (4)], t is negative when the mean increases between adjacent samples; and F is greater than one when the variance decreases between adjacent samples. Thus, for Fig. 7 at least, the preferred regime that produces both first-order and second-order nonstationarity is for the mean to increase while the variance simultaneously decreases.

Such behavior is evidence of coherent structure—essentially temperature ramps (Antonia et al. 1979; Phong-anant et al. 1980; Kikuchi and Chiba 1985)—in the atmospheric surface layer. Antonia and Chambers (1978), Antonia et al. (1979, 1982), and Phong-anant et al. (1980) describe such ramps in the unstably stratified surface layer; while Kikuchi and Chiba (1985) and Revelle (1993) report ramps in the stably stratified surface layer, which is the situation represented in
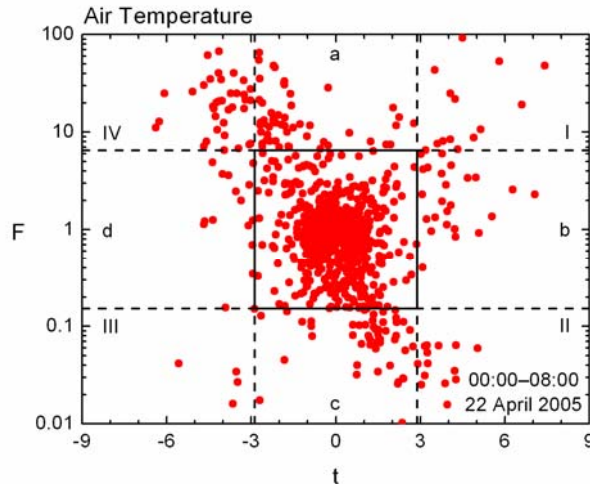
Fig. 7. The t and F statistics for the air temperature data in Fig. 5 are displayed as a scatter plot. Markers within the central box are within both t and F 99% confidence bands and would indicate stationary data. Markers in sectors a and b indicate first-order stationary but second-order nonstationary data. Markers in sectors b and d indicate first-order nonstationary but second-order stationary data. Markers in sectors I–IV indicate data that are both first-order and second-order nonstationary.
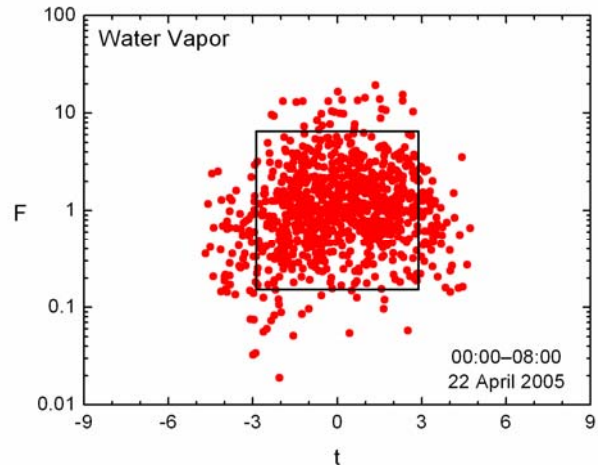

Fig. 8. As in Fig. 7, but this shows the t and F statistics for water vapor density from Fig. 6. This plot would have the same sectors delineated in Fig. 7, but we omit the dashed lines for less cluttered viewing. Markers in the central box indicate strict stationarity.

Figs. 5–8. Furthermore, in our case, the ramps seem to be evidence of coherent "sweeps" (e.g., Högström and Bergström 1996) that bring relatively warm air from aloft down to the surface to offset the radiative losses.

While Figs. 5 and 7 suggest that the temperature signal for 0000 to 0800 hours on 22 April was nonstationary, our similar analysis shows that temperature is better behaved for 0800 hours through midnight. In Fig. 4, the t and F statistics for temperature make fewer excursions outside their 99% confidence bands. During this period, only 2.3% of the t values and only 2.6% of the F values stray outside the 99% confidence bands. These extreme values, however, generally cluster and, thus, indicate isolated nonstationary events within a signal that is basically stationary. In fact, in only 0.3% of the samples from 0800 hours through midnight do t and F simultaneously exceed their respective 99% confidence limits. Based on this more restrictive definition of nonstationarity, we might conclude that the temperature trace for 0800 to 2400 hours on 22 April in Fig. 3 represents stationary

conditions despite the obvious rapid forcing by the clouds.

Figure 8, the scatter plot of t and F for water vapor density for 0000 to 0800 hours on 22 April, contrasts with Fig. 7. Here, 13.6% of the t statistics fall outside the 99% confidence band— that is, they fall in sectors I–IV and b and d. But only 6.3% of the F statistics fall outside the 99% confidence band. Thus, as with Fig. 7, Fig. 8 shows ample evidence of first-order and second-order nonstationarity. But only a bit more than 1% of the samples (10 of 959) in Fig. 8 exhibit first-order and second-order nonstationarity simultaneously. Consequently, with this more restrictive definition of nonstationarity, we might conclude that the water vapor trace in Fig. 6 is essentially stationary.

Moreover, no samples fall in sector IV, which was the most populated of the simultaneously nonstationary temperature cases in Fig. 7. No samples fall in sector I either, and only one sample falls in Sector II. Thus, in contrast to Fig. 7, 9 of the 10 cases for which t and F are simultaneously outside their 99% confidence bands fall in sector

III. Here, both the mean and the variance increase significantly between adjacent samples.

For the other 16 hours on 22 April, from 0800 to 2400 hours (see Figs. 3 and 4), only 2.1% of the t statistics and only 3.4% of the F statistics are outside their respective 99% confidence bands. Again, since these are 1% significance tests, we would still be concerned about nonstationarity in the water vapor signal. But as with air temperature, the excursions outside the 99% confidence bands for 0800 to 2400 hours, especially for t, occur in clusters. Furthermore, during this 16-hour period, only in 0.3% of the total samples do the extremes in t and F occur simultaneously.

5. CONCLUSIONS

Our original hypothesis was that changes in cloud forcing immediately affect the surface temperature and, thus, the temperature of the near-surface atmosphere and, perhaps, other near-surface meteorological variables. Our two examples of day-long traces of the radiative forcing and the responses in surface temperature and in near-surface air temperature and humidity (Figs. 2 and 3) confirm this scenario. The surface temperature responds almost immediately and significantly to rapid changes in the incoming shortwave and longwave radiation that are associated with changing cloud conditions. The near-surface air temperature also quickly follows suit because it is closely coupled to the surface through the sensible heat flux. We also see cases when the near-surface water vapor density also responds to this cloud forcing—presumably through changes in the latent heat flux from the surface or because of changes in boundary layer mixing.

The second part of our hypothesis was that changes in cloud forcing lead to nonstationarity in the turbulent properties of the near-surface atmosphere. We looked for such nonstationarity in the air temperature and the water vapor density by introducing new analysis techniques. We first used the Time Dependent Memory Method (Treviño and Andreas 2000) to separate mean and fluctuating parts of the air temperature and humidity signals. TDMM is designed specifically to pull means and variances out of a signal that is presumed to be nonstationary.

With the means and variances from TDMM, we computed two familiar statistics, t and F, every 30 s but applied them for the first time to the problem of identifying first-order and second-order nonstationarity. Testing at the 1% significance level, we found in both our examples that the midnight-to-sunrise temperature and water vapor signals were severely nonstationary. Micrometeorologists have said for a long time that nighttime conditions are often nonstationary; our statistics quantify that maxim.

The daylight data, however, are less conspicuously nonstationary according to our t and F tests despite examples selected with frequent changes in cloud forcing. We see short clusters of nonstationarity associated with the most extreme changes in cloud forcing. But the rapid, small changes in incoming shortwave radiation in Fig. 3 that we associated with varying cirrus clouds do not produce severe nonstationarity.

Perhaps Monin-Obukhov similarity functions measured during the day under conditions of variable cloudiness have not been seriously degraded by nonstationarity. On the other hand, our analysis suggests that any similarity functions measured at night over terrestrial surface experiencing diurnal forcing likely suffer severely from nonstationarity. In other words, nonstationarity may explain the wide range in Monin-Obukhov similarity functions that apply to stable stratification (e.g., Andreas 2002).

6. ACKNOWLEDGMENTS

7. REFERENCES

Andreas, E. L, 1988: Estimating averaging times for point and path-averaged measurements of turbulence spectra. *J. Appl. Meteor.,* **27**, 295-304.

——, 2002: Parameterizing scalar transfer over snow and ice: A review. *J. Hydrometeor.*, **3**, 417–432.

——, R. J. Hill, J. R. Gosz, D. I. Moore, W. D. Otto, and A. D. Sarma, 1998: Statistics of surface-layer turbulence over terrain with metre-scale heterogeneity. *Bound.-Layer Meteor.*, **86**, 379–408.

——, C. W. Fairall, P. O. G. Persson, and P. S. Guest, 2003: Probability distributions for the inner scale and the refractive index structure

parameter and their implications for flux averaging. *J. Appl. Meteor.*, **42**, 1316–1329.

——, C. A. Geiger, K. J. Claffey, G. Treviño, and C. C. Ryerson, 2006: Rapid forcing of the surface and near-surface atmosphere. Preprints, *10th Symp. on Integrated Observing and Assimilation Systems for the Atmosphere, Oceans, and Land Surfaces*, Atlanta, GA, Amer. Meteor. Soc., CD-ROM 4.2, 12 pp.

Antonia, R. A., and A. J. Chambers, 1978: Note on the temperature ramp structure in the marine surface layer. *Bound.-Layer Meteor.*, **15**, 347–355.

——, ——, C. A. Friehe, and C. W. Van Atta, 1979: Temperature ramps in the atmospheric surface layer. *J. Atmos. Sci.*, **36**, 99–108.

——, ——, and E. F. Bradley, 1982: Relationships between structure functions and temperature ramps in the atmospheric surface layer. *Bound.-Layer Meteor.*, **23**, 395–403.

Foken, Th., and B. Wichura, 1996: Tools for quality assessment of surface-based flux measurements. *Agric. Forest Meteor.*, **78**, 83–105.

Högström, U., 1996: Review of some basic characteristics of the atmospheric surface layer. *Bound.-Layer Meteor.*, **78**, 215–246.

——, and H. Bergström, 1996: Organized turbulence structures in the near-neutral atmospheric surface layer. *J. Atmos. Sci.*, **53**, 2452–2464.

Johansson, C., A.-S. Smedman, U. Högström, J. G. Brasseur, and S. Khanna, 2001: Critical test of the validity of Monin-Obukhov similarity during convective conditions. *J. Atmos. Sci.*, **58**, 1549–1566.

Kaimal, J. C., and J. J. Finnigan, 1994: *Atmospheric Boundary Layers Flows: Their Structure and Measurement*. Oxford University Press, 289 pp.

——, and J. E. Gaynor, 1991: Another look at sonic thermometry. *Bound.-Layer Meteor.*, **56**, 401–410.

——, ——, H. A. Zimmerman, and G. A. Zimmerman, 1990: Minimizing flow distortion errors in a sonic anemometer. *Bound.-Layer Meteor.*, **53**, 103–115.

Kikuchi, T., and O. Chiba, 1985: Step-like fluctuations associated with inverted ramps in the stable surface layer. *Bound.-Layer Meteor.*, **31**, 51–63.

Klipp, C. L., and L. Mahrt, 2004: Flux-gradient relationship, self-correlation and intermittency in the stable boundary layer. *Quart. J. Roy. Meteor. Soc.*, **130**, 2087–2103.

Kristensen, L., J. Mann, S. P. Oncley, and J. C. Wyngaard, 1997: How close is close enough when measuring scalar fluxes with displaced sensors? *J. Atmos. Oceanic Technol.*, **14**, 814–821.

Lenschow, D. H., J. Mann, and L. Kristensen, 1994: How long is long enough when measuring fluxes and other turbulence statistics? *J. Atmos. Oceanic Technol.*, **11**, 661–673.

Lumley, J. L., and H. A. Panofsky, 1964: *The Structure of Atmospheric Turbulence.* Interscience, 239 pp.

Mahrt, L., 1998: Flux sampling errors for aircraft and towers. *J. Atmos. Oceanic Technol.*, **15**, 416–429.

Phong-anant, D., R. A. Antonia, A. J. Chambers, and S. Rajagopalan, 1980: Features of the organized motion in the atmospheric surface layer. *J. Geophys. Res.*, **85**, 424–432.

Priestley, M. B., 1981: *Spectral Analysis and Time Series.* Academic Press, 890 pp.

Revelle, D. O., 1993: Chaos and "bursting" in the planetary boundary layer. *J. Appl. Meteor.*, **32**, 1169–1180.

Roth, M., and T. R. Oke, 1995: Relative efficiencies of turbulent transfer of heat, mass, and momentum over a patchy urban surface. *J. Atmos. Sci.*, **52**, 1863–1874.

Sreenivasan, K. R., A. J. Chambers, and R. A. Antonia, 1978: Accuracy of moments of velocity and scalar fluctuations in the atmospheric surface layer. *Bound.-Layer Meteor.*, **14**, 341–359.

Treviño, G., and E. L Andreas, 2000: Averaging intervals for spectral analysis of nonstationary turbulence. *Bound.-Layer Meteor.*, **95**, 231–247.

Vickers, D., and L. Mahrt, 1997: Quality control and flux sampling problems for towers and aircraft data. *J. Atmos. Oceanic Technol.*, **14**, 512–526.

Wyngaard, J. C., 1973: On surface-layer turbulence. *Workshop on Micrometeorology*, D. A. Haugen, Ed., Amer. Meteor. Soc., 101–149.